Supporting Information

Plasmonic Chiral Metamaterials with Sub-10 nm Nanogaps

Wei Zhang,[1] Bin Ai,[2] Panpan Gu,[3] Yuduo Guan,[1] Zengyao Wang,[1,4] Zifan Xiao,[1] Gang Zhang[1]*

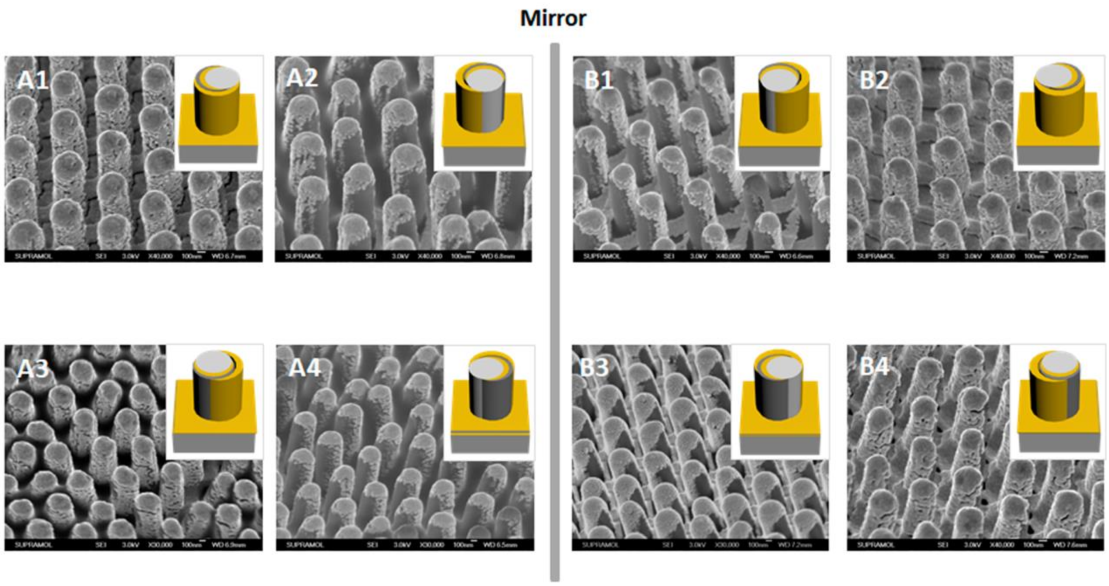

Figure S1. The 45° titling SEM images of (A) Left-handed and (B) Right-handed three metal films deposited samples viewed from different directions (A1-A4, B1-B4). The insets are the schematics images of the corresponding observation. The schematic diagram does not reflect the deposition shadow effect of the substrate in order to simplify the model.

We performed the distance measurement based on a large amount of data statistics analysis in high resolution SEM. Serveral SEM images with an area of 14 μm^2 were selected for gap-width measurement, and the final *G* refers to the average gap-width. The corresponding probability distribution histogram of gap-width is shown in Figure S2, which is kept to one decimal place.

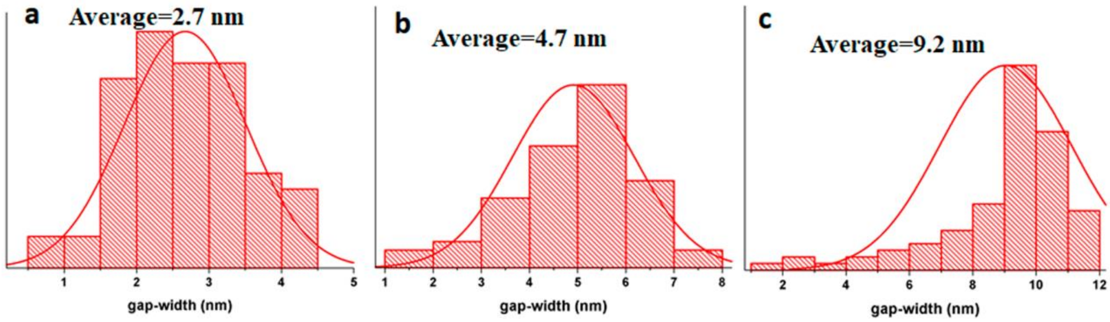

Figure S2. Probability distribution histogram of different gap-width with the average gap-width of (a) G = 2.5 nm, (b) G = 5 nm and (c) G = 10 nm.

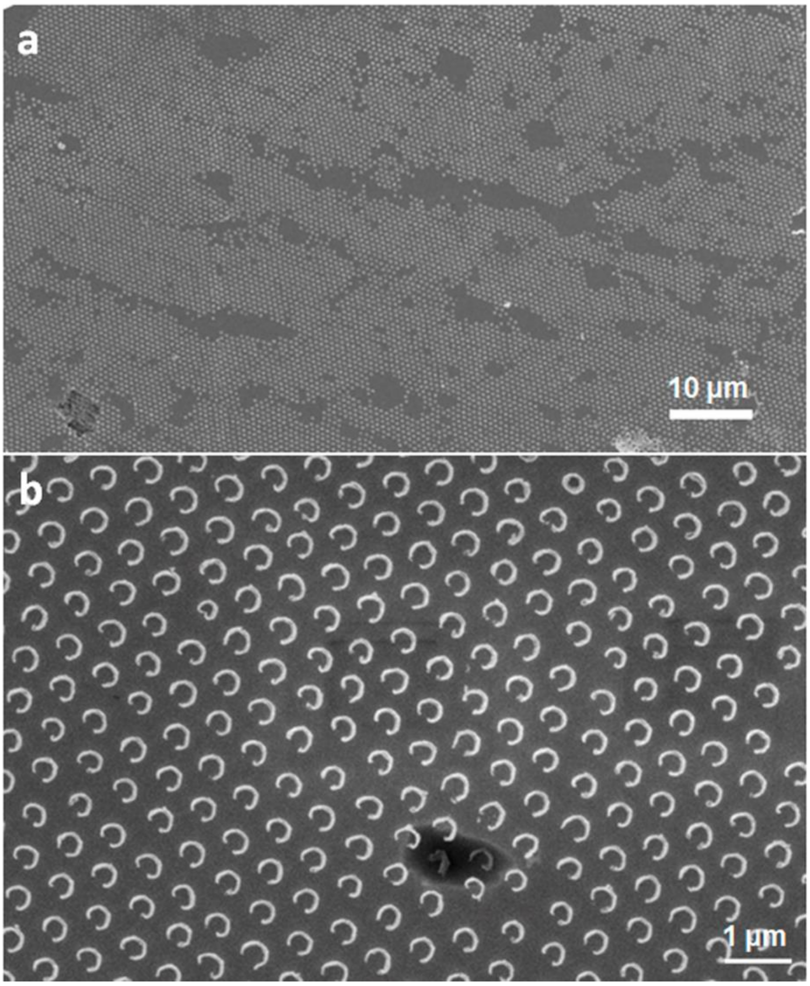

Figure S3. SEM image of large-area R-chiral nanogap with G = 5 nm.

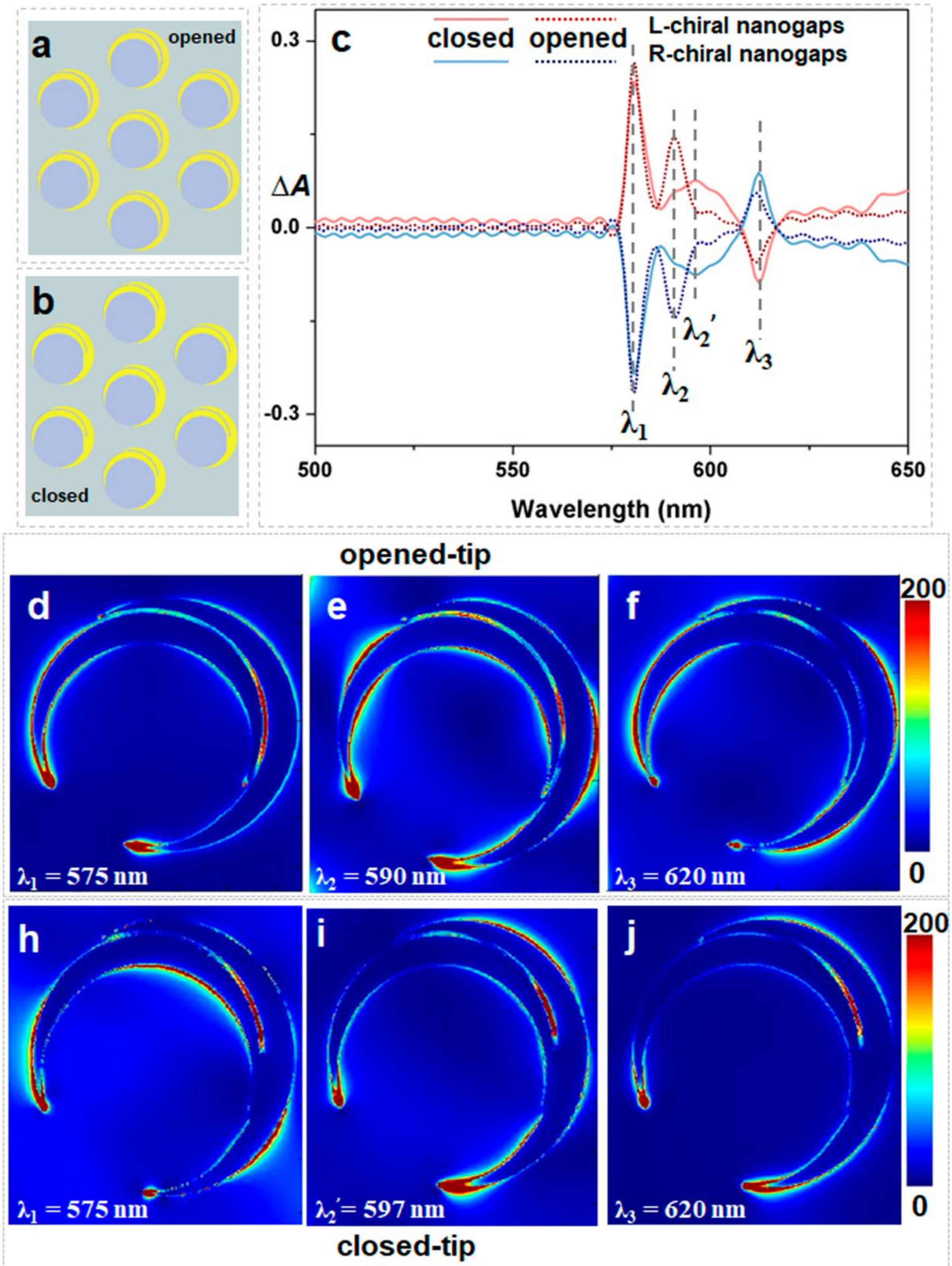

Figure S4. The models of the (a) closed-tip and (b) opened-tip chiral nanogaps used in FDTD. (c) Calculated absorption spectra difference of closed and opened chiral nanogaps. Simulated electric field distribution $|E|^2/|E_0|^2$ of opened-tip R-chiral nanogaps with G = 5 nm at the wavelength of λ = (d) 575 nm, (e) 590 nm, (f) 620 nm; the closed-tip R-chiral nanogaps at λ = (h) 575 nm, (i) 597 nm, (j) 620 nm.

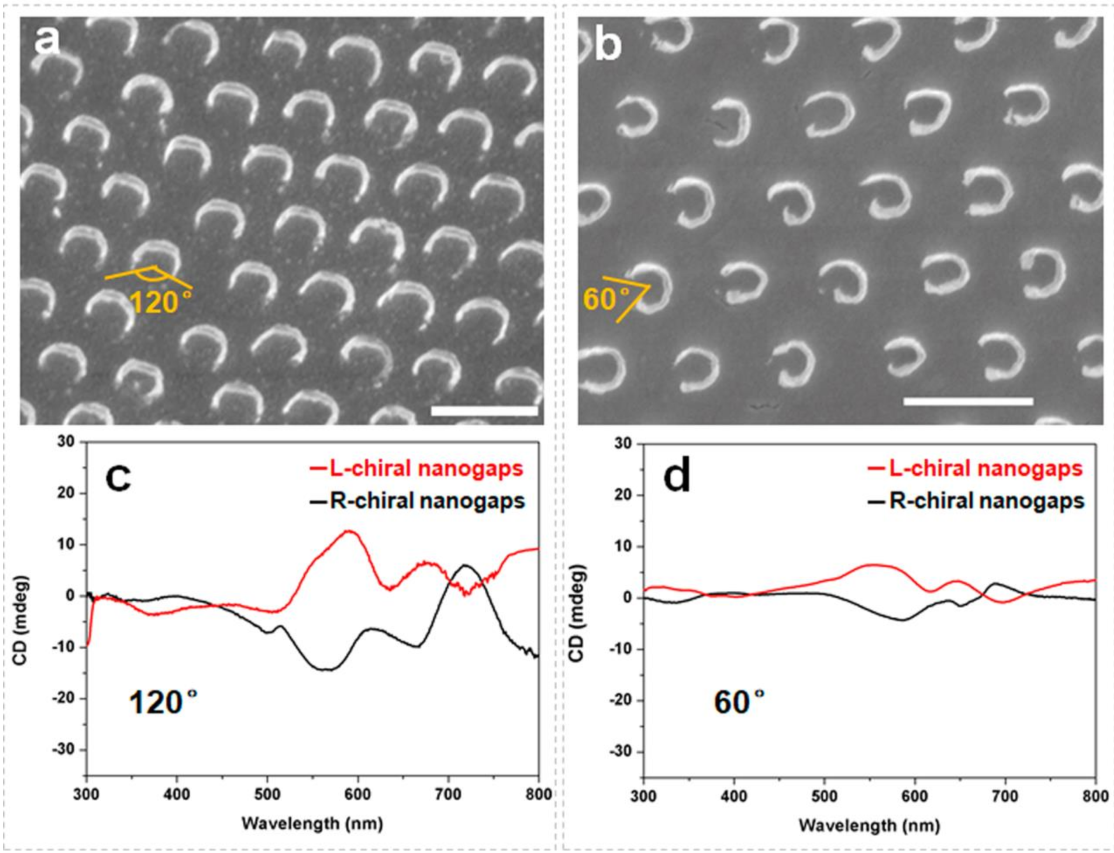

Figure S5. SEM images (a, b) and experimental CD spectra (c and d) of chiral nanogaps with different opening angle φ = 120° and 60°.

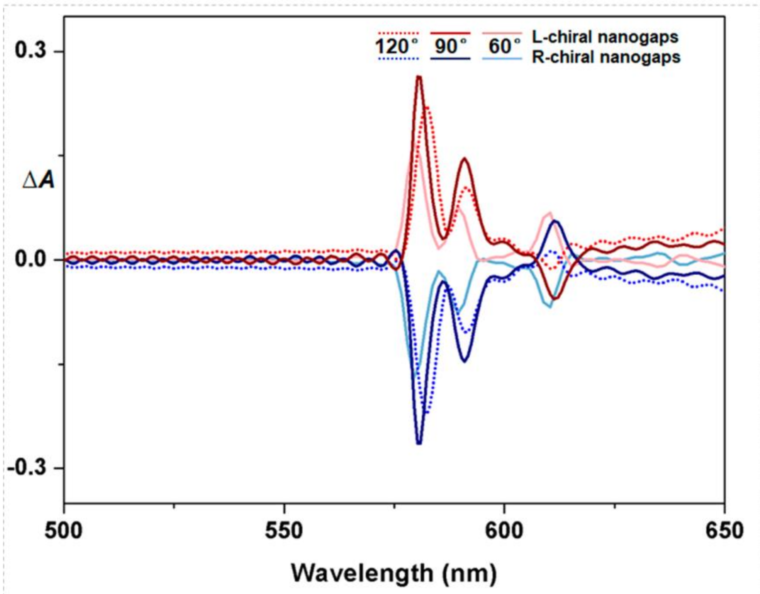

Figure S6. calculated absorption difference spectra of chiral nanogaps with different opening angle φ = 120°, 90° and 60°.

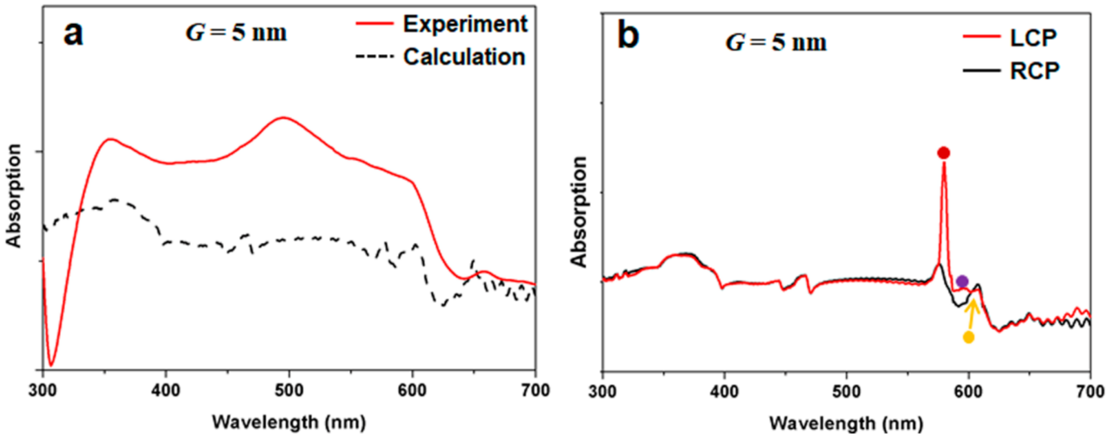

Figure S7. (a) Calculated and experimental absorption spectra of L-chiral nanogaps with G = 5 nm. (b) Calculated absorption spectra under CPL of L-chiral nanogaps with G = 5 nm.

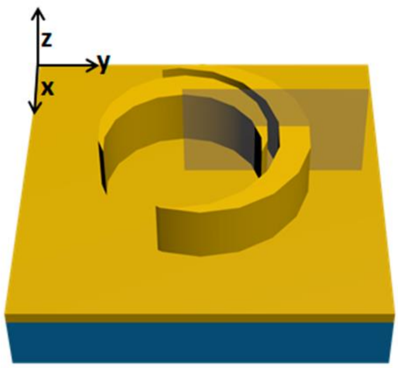

Figure S8. The schematic of movie monitor in the *x*-*z* plane crossing the nanogap.

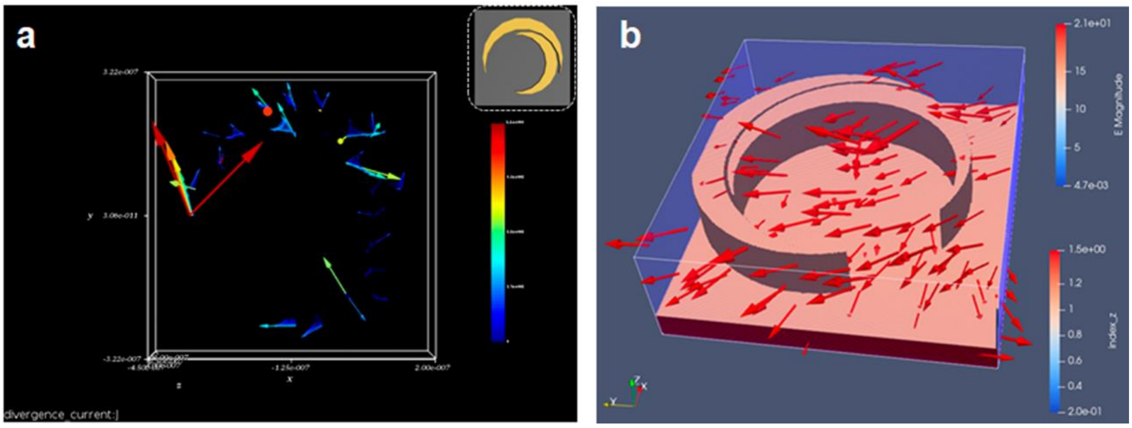

Figure S9. (a) The original calculated near field current distribution at the wavelength (a) λ = 575 nm of L-chiral nanogaps with G = 5 nm by FDTD. (b) Illustration of (a) by paraview.

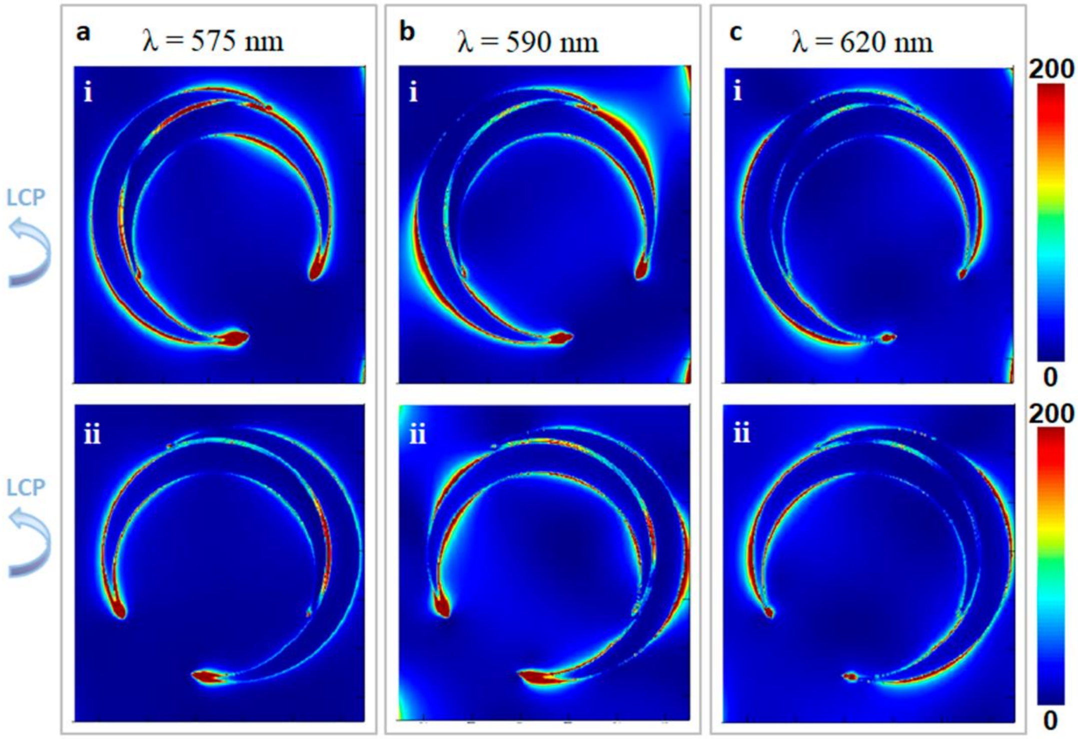

Figure S10. Calculated electric field distribution at the wavelength (a) λ = 575 nm, (b) λ = 595 nm, (c) λ = 620 nm of (i) L- and (ii) R-chiral nanogaps with G = 5 nm.

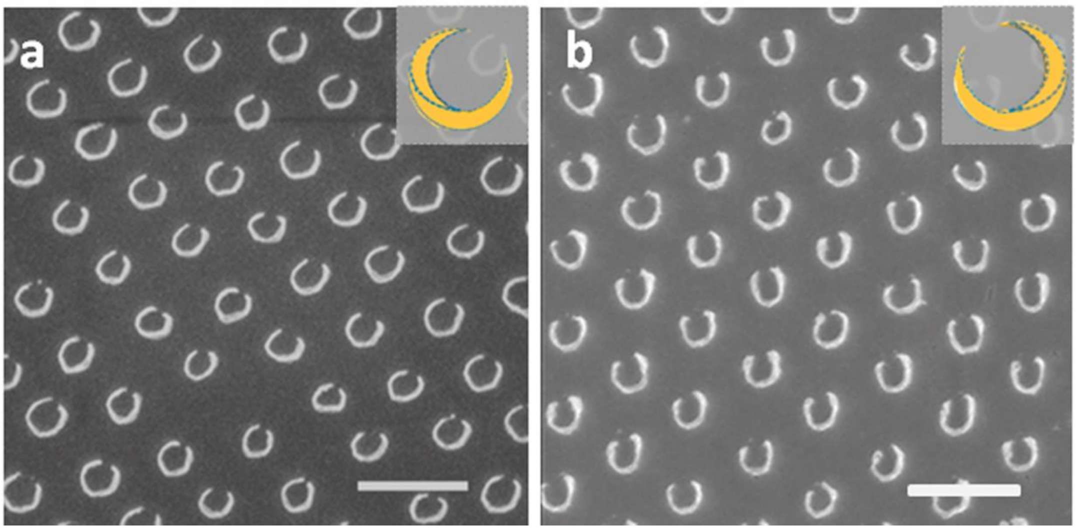

Figure S11. SEM images of (a) L- and (b) R-crescent nanowires without nanogap. Scale bar: 1 μm.

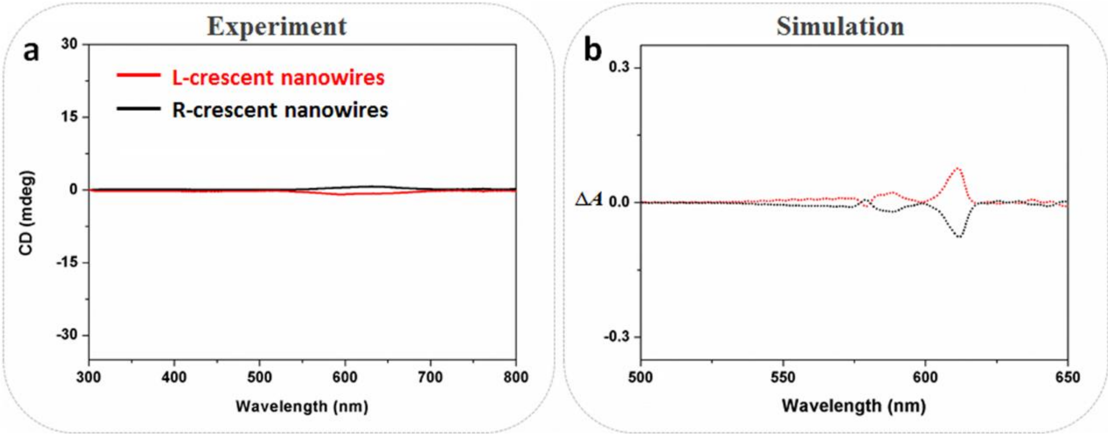

Figure S12. (a) Experimental CD spectra and (b) calculated absorption difference of L- and R-crescent nanowires without nanogap.

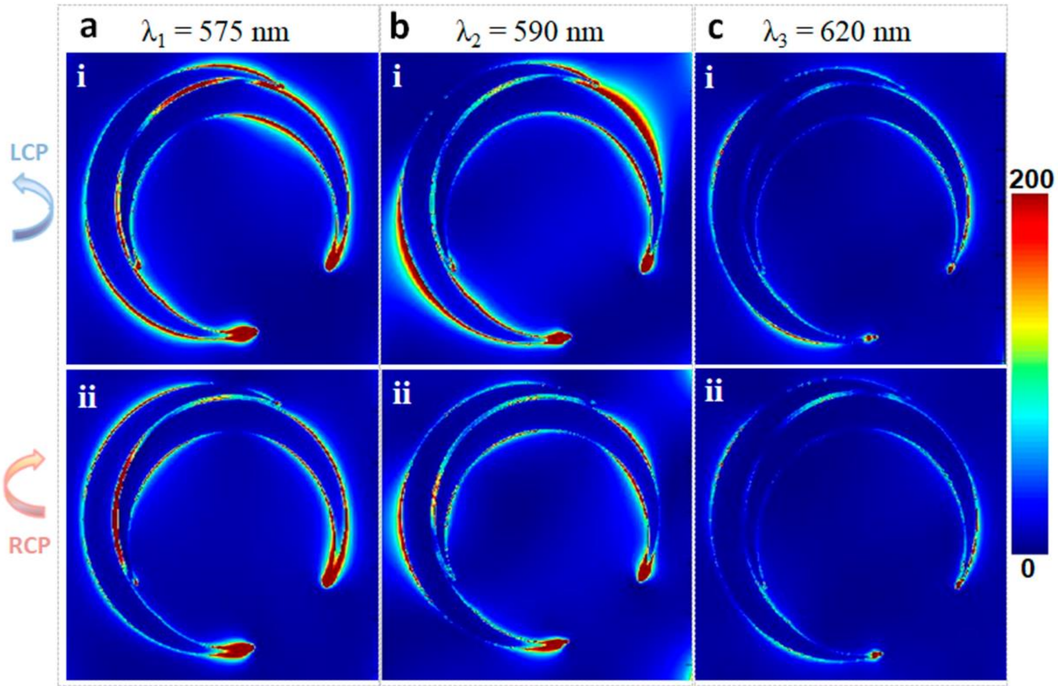

Figure S13. Calculated electric field distribution of L-chiral nanogaps with $G = 5$ nm illuminated by (i) LCP and (ii) RCP at the different wavelength of (a) $\lambda = 575$ nm, (b) $\lambda = 590$ nm, and (c) $\lambda = 620$ nm.

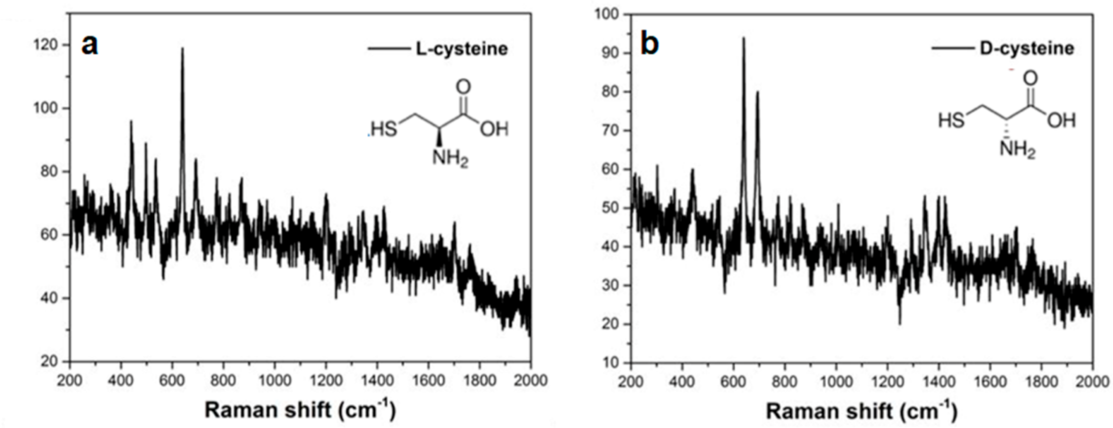

Figure S14. Typical Raman spectra of (a) pure L-cysteine and (b) pure D-cysteine recorded on Au film.

REFERENCES

(1) Zhang, W.; Gu, P.; Wang, Z.; Ai, B.; Zhou, Z.; Zhao, Z.; Li, C.; Shi, Z.; Zhang, G. Integrated "Hot Spots": Tunable Sub-10 nm Crescent Nanogap Arrays. *Adv. Opt. Mater.* **2019**, *7*, 1901337.

(2) Kuang, X.; Ye, S.; Li, X.; Ma, Y.; Zhang, C.; Tang, B. A New Type of Surface-Enhanced Raman Scattering Sensor for the Enantioselective Recognition of D/L-Cysteine and D/L-Asparagine Based on a Helically Arranged Ag NPs@Homochiral MOF. *Chem. Commun.* **2016**, *52*, 5432-5435.